A Neural-Network-Based Controller for Piezoelectric-Actuated Stick-Slip Devices

Long Cheng, *Senior Member*, *IEEE*, Weichuan Liu, Chenguang Yang, Senior Member, *IEEE*, Tingwen Huang, *Member*, Zeng-Guang Hou, *Senior Member*, *IEEE*, *IEEE*, and Min Tan

***Abstract*—Piezoelectric-actuated stick-slip device (PASSD) is a highly promising equipment that composed of one end-effector, one piezoelectric actuator (PEA) and one driving object adhered to the PEA. Since the end-effector can slip on the surface of the driving object, the PASSD is capable of realizing the macro-level motion with the micro-level precision. Due to the following two reasons: (1) the complicated relative motion between the end-effector and the driving object, and (2) the inherent hysteresis nonlinearity in the PEA, the ultraprecision displacement control of the end-effector of PASSDs raises a real challenge, which is rarely reported in the literature. Towards solving this challenge, a neural network based controller is proposed in this paper. First, a neural network based model is proposed to capture the relative motion between the end-effector and the driving object. Second, a neural network based inversion model is developed to on-line calculate the desired position of the PEA under the predesigned reference of the end-effector. Third, a dynamic linearized neural network based model predictive control method, which can effectively handle the hysteresis nonlinearity, is employed to implement the displacement control of the PEA, which finally results in an overall high-precision controller of the end-effector. Finally, a PASSD prototype has been implemented and tested through experimental studies to demonstrate the effectiveness of the proposed approach.**

***Index Terms*—Stick-slip, piezoelectric actuator, end-effector, neural network.**

I. Introduction

RECENTLY, the nano/micro-level positioning becomes a vital technology in many ultra-precision applications such as the computer component [1], the micro-manipulation system [2], and the atomic force microscope [3]. Among these applications, the piezoelectric actuator (PEA) is the kernel positioning component owing to its high precision and fast response characteristics [4]. However, the limited motion range is an unavoidable issue of PEAs [5]. Therefore, how to realize a long range motion with a relatively high precision is a challenging task in the literature. Towards this challenge, the piezoelectric-actuated stick-slip device (PASSD) is one most widely adopted approach because of its theoretically unlimited motion and high positioning precision [6]. The working principle of PASSDs is briefly introduced in the following paragraph.

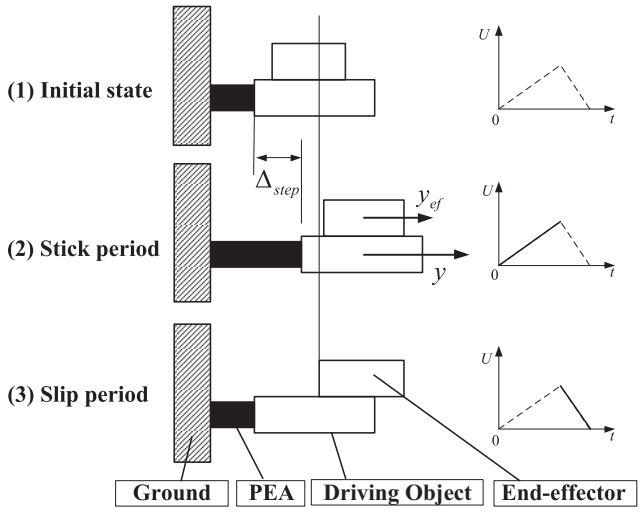

Fig. 1. The stick-slip principle of PASSDs.

The PASSD is usually composed of one PEA, one driving object adhered to the PEA, and one end-effector [7], as shown in Fig. 1. The end-effector is driven by the friction force generated from the relative motion between the end-effector and the driving object. This friction-based driven approach is the so-called stick-slip mode which is a widely adopted driven manner in PASSDs. The stick-slip mode usually includes three parts: the initial state, the stick period, and the slip period [7], [8].

1) *The initial state*: in the initial phase, there is no voltage applied to the PEA. The end-effector is horizontally placed on the upper surface of the driving object. Both the end-effector and the driving object stay at their initial positions, respectively.
2) *The stick period*: in the stick period, the input voltage of the PEA is increased slowly, which pushes the driving object rightward to a displacement Δ_{step} with a low acceleration. An external force on the end-effector, which

This work was supported in part by the National Natural Science Foundation of China under Grants 61422310, 61633016, 61370032 and 61421004; the Beijing Natural Science Foundation under Grant 4162066; Royal Society Newton Mobility Grant IE150858 and International Exchanges Grant IE170247; and the Qatar National Research Fund under National Priority Research Project NPRP 9 166-1-031.

L. Cheng, W. Liu, Z.-G. Hou and M. Tan are with the State Key Laboratory of Management and Control for Complex Systems, Institute of Automation, Chinese Academy of Sciences, Beijing 100190, China. L. Cheng is also with the University of Chinese Academy of Sciences.

C. Yang is with Zienkiewicz Centre for Computational Engineering, Swansea University, SA1 8EN, UK.

T. Huang is with with the Texas A&M University at Qatar, Doha 23874, Qatar. Corresponding Author: tingwen.huang@qatar.tamu.edu.

depends on the end-effector's mass and the PEA's acceleration, is smaller than the static friction force between between the end-effector and the driving object. Therefore, the end-effector "sticks" with the driving object and moves along with it to a same displacement Δ_{step}.

3) *The slip period*: in the slip period, the input voltage of the PEA is rapidly decreased to zero. Then the PEA pulls the driving object backward quickly with a high acceleration. In this period, the external force on the end-effector is greater than the friction force between the end-effector and the driving object. The end-effector "slips" on the surface of the driving object.

Based on the above introduction, it can be seen that the stick-slip actuation mode is mainly determined by two factors: (1) the relative motion between the end-effector and the driving object; and (2) the displacement control of the PEA. The first factor is highly dependent on the friction. In the literature, there are some friction models which can be used for PASSDs such as the Coulomb model, the viscous model, the Dahl model, the LuGre model and the elasto-plastic model [9]. However, due to their complicated nonlinearities, these friction models are barely considered in the controller design of the end-effector. For the second factor, the positioning accuracy can be seriously deteriorated by the inherent hysteresis nonlinearity of PEAs. To deal with the hysteresis nonlinearity of PEAs, there are various control methods in the literature, such as the inversion-based methods [10], [11], the sliding mode control methods [12]–[15], the active disturbance rejection control [16], [17], and some intelligent control methods [18]–[23]. Although these methods are successfully applied in the control of PEAs, to the best of the authors' knowledge, there is no such an attempt of using these advanced control algorithms to deal with the hysteresis nonlinearity in PASSDs. Therefore, how to effectively control the PASSD is still a challenging task and it is seldom studied in the literature [24], [25]. The most classical control method of PASSDs is the proportional control law without considering the friction and the hysteresis nonlinearity [9]. For this method, it simply applies the proportional control law to the PEA according to the tracking error of the end-effector, which cannot lead to a satisfactory control performance. A modified voltage/frequency proportional control strategy is presented for the control performance improvement in [26]. Unfortunately, the fundamental limitation in the proportional control approach still exists. To further improve the control performance of the proportional controller, the iterative learning control idea is adopted in [27]. However, the control parameters have to be re-learned once the desired reference of the end-effector is changed and it is hard to ensure that the friction during each learning period is the same. In [28], a hybrid charge control method for PASSDs is developed to increase the slip speed. Since the charge control is used, the effect of the hysteresis nonlinearity can be avoided. However, the friction effect is still ignored. In [29], the velocity of the end-effector is adopted to compensate the vibration of PASSDs, however, an accurate velocity estimation is difficult to be realized in practice. By reviewing the very limited literature, it is evident that the high-precision control of PASSDs is far away from being fully solved, which gives the motivation of the study conducted here.

This paper proposes a neural network based control method for the high precision positioning of PASSDs. The proposed controller includes two types of control phases: the one-step control phase (the coarse positioning) and the sub-step control phase (the fine positioning). To achieve a satisfactory positioning accuracy in the sub-step control phase, the relative motion between the end-effector and the driving object is first modeled by a neural network based on the identification approach (this neural network model is called the end-effector's motion estimator). The advantages of this identification based method are: (1) the specific parameters in the friction model cannot be known a prior; (2) different friction models can be approximated by this identification based approach; and (3) the complicated analysis and computation for determining the end-effector's motion by friction can be avoided. Second, an inversion of the end-effector's motion estimator is obtained by using the neural network technique as well. With this inversion model, the desired position of the driving object can be determined by the predesigned reference of the end-effector. Third, the model predictive control method proposed in [30] is employed to control the PEA to let the driving object reach the desired position. This model predictive controller is able to handle the hysteresis nonlinearity well. Finally, a PASSD prototype device is developed to verify the proposed modeling and control methods. The experiments results show that the relative motion between the end-effector and the driving object can be captured by the proposed neural network model well and a high positioning accuracy of PASSDs has been achieved by the proposed controller. In the literature, there is one recent paper addressing the control of PASSDs using the predictive control approach [31], while it is assumed that there is no relative motion between the end-effector and the driving object in the sub-step control phase. Therefore, the high precision control of PASSDs is transformed into the high precision control of the PEA. However, it is difficult to maintain the zero relative motion in some fast positioning scenarios and the consideration of the relative motion between the end-effector and the driving object is more reasonable and necessary in practice.

The rest of this paper is organized as follows: in Section II, some preliminary results on the control principle of PASSDs and the model predictive controller for PEAs are provided; Section III proposes the neural network based end-effector's motion estimator and its inversion and explains how to achieve the high precision control of PASSDs; Section IV presents details of the PASSD prototype and conducts experiments to verify the proposed modeling and control methods; and the conclusion remarks are given in Section V.

II. Preliminaries

A. Control Paradigm of PASSDs

By the stick-slip principle of PASSDs shown in Fig. 1, the control paradigm of PASSDs is usually divided into two phases: the one-step control phase and the sub-step control phase.

- **One-step control phase**: this phase is composed of one stick period and one slip period. By repeating the one-step control phase, the stick period and the slip period appear cyclically, and the end-effector is driven to continuously move on the surface of the driving object. Theoretically speaking, the end-effector could achieve a unlimited displacement as long as the length of the driving object is sufficiently large. And the positioning resolution of the end-effector is the movement length Δ_{step} of the end-effector in each one-step control phase [1], which is a very coarse positioning. For example, if the required motion range L_d is relatively large, the PASSD only needs to operate the "one-step control phase" for $\left\lfloor \frac{L_d}{\Delta_{step}} \right\rfloor$ times ($\lfloor x \rfloor$ denotes the largest integer smaller than x). After completing the "one-step control phase", the PASSD enters the "sub-step control phase" and the end-effector only needs to move forwards a length of $(L_d - \left\lfloor \frac{L_d}{\Delta_{step}} \right\rfloor \Delta_{step})$, where the advanced control approach should be used in the "sub-step control phase" to guarantee the high positioning accuracy of the end-effector.
- **Sub-step control phase**: in this phase, the end-effector is controlled to the desired position with the required precision. To this end, one possible way is to move the PEA with a very small acceleration such that there is no relative motion between the end-effector and the PEA (*i.e.*, the stick period). In this way, the positioning accuracy of the end-effector equals to the positioning accuracy of the PEA. Based on this idea, some preliminary results have been obtained in [31]. However, to maintain the zero relative motion, the PEA must move with a very low acceleration, which is not acceptable in some applications with strict time requirements. Another way is to allow the non-zero relative motion between the end-effector and the PEA. In this way, the relationship between the motion of the end-effector and the motion of the driving object should be modeled first. Then the desired position of the driving object can be calculated by using this relationship and the predesigned reference of the end-effector. After that, some advanced control methods of PEAs can be employed to drive the driving object to this desired position in a fast manner.

The overall control paradigm of PASSDs is shown in Fig. 2. First, the sawtooth signal is used as the input voltage of the PEA and then the PASSD enters the "one-step control phase" repeatedly. At the end of each one-step control phase, check whether the positioning error of the end-effector is smaller than the movement length of the end-effector during the one-step control phase. If no, continue applying the sawtooth signal to the PEA. If yes, switch to the sub-step control phase to achieve the "accurate" positioning of the end-effector.

[1]In practice, the movement length of the end-effector in each "one-step control phase" may be time-variant because of the different friction coefficients. In some particular cases, the movement length of the end-effector can even be reduced intentionally to obtain an increased positioning resolution [8]. However, this does not effect the final positioning accuracy because the one-step control phase only gives a "coarse" positioning of the end-effector.

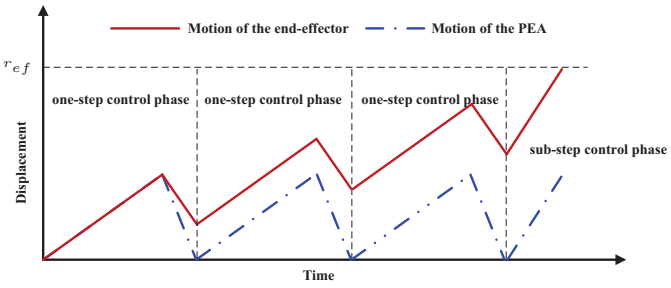

Fig. 2. The control paradigm of PASSDs.

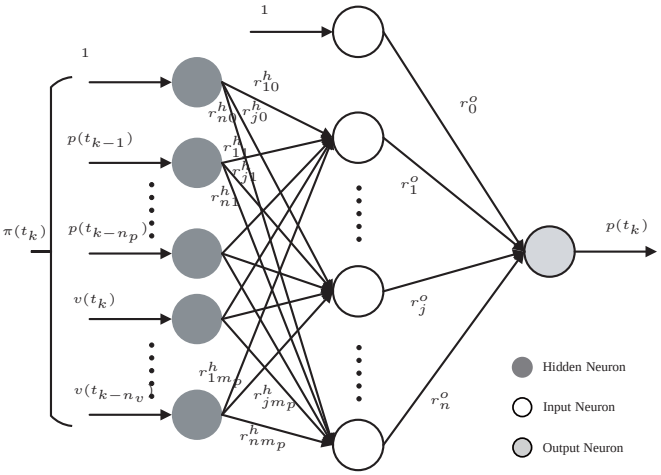

Fig. 3. The structure of the feedforward neural network defined by (2).

In the sub-step control phase, it can be seen that the positioning control of PEAs is one crucial technique for PASSDs. Among the advanced control algorithms of PEAs, this paper employs the dynamic linearized neural network based model predictive control method proposed in [30] because this method requires no calculation of the inversion of hysteresis and has a satisfactory control performance by experiment validations. The next subsection gives a brief introduction to this model predictive control method.

B. Dynamic Linearized Neural Network Based Model Predictive Controller for PEAs

Since the driving object is rigidly adhered to the PEA, there is no relative motion between them. Hence if we use the motion of the point connecting the driving object and the PEA to describe the motion of the driving object, the motion (displacement) of the driving object is treated same as the one of the PEA throughout this paper. Therefore, the driving object can be positioned with a desired precision as long as the PEA is controlled well.

To design the model predictive controller for PEAs, the input-output model of PEAs should be obtained first, which can be identified by using the following "nonlinear auto-regressive moving average with exogenous inputs" structure

$$p(t_k) = \mathscr{P}(\pi(t_k)), \tag{1}$$

where $\pi(t_k) = [p(t_{k-1}), \cdots, p(t_{k-n_p}), v(t_k), \cdots, v(t_{k-n_v})]$, $p(t_k)$ and $v(t_k)$ are the displacement and input voltage of PEAs at the kth sampling interval, respectively; integers n_p and n_v are the corresponding maximum lags for $p(t_k)$ and $v(t_k)$. $\mathscr{P}(\cdot)$ is a nonlinear mapping to be determined. Since the input-output data pair $(p(t_k), v(t_k))$ can be physically measured, $\mathscr{P}(\cdot)$ can be approximated by the following feedforward neural network whose structure is given in Fig. 3

$$\mathscr{P}(\pi(t_k)) = \sum_{j=1}^{n} r_j^o \sigma(\sum_{i=1}^{m_p} r_{ji}^h \pi_i(t_k) + r_{j0}^h) + r_0^o, \quad (2)$$

where $m_p = n_p + n_v + 1$ is the number of neurons in the input layer, and n is the number of neurons in the hidden layers. r_j^o is the weight between the jth hidden neuron and the output neuron; r_0^o is the bias of the output neuron; r_{ji}^h is the weight between the ith input neuron and the jth hidden neuron; r_{j0}^h is the bias of the jth hidden neuron. These parameters are trained by the Levenberg-Marquardt algorithm (see Chapter 10, pp. 258–262, [32]) based on the training data set $(\pi(t_k), p(t_k))$. $\pi_i(t_k)$ denotes the ith entry of $\pi(t_k)$. The activation function of hidden neurons is the tangent sigmoid function

$$\sigma(x) = \frac{e^{2x} - 1}{e^{2x} + 1}, \quad (3)$$

while the activation functions of input neurons and the output neuron are all the unit mapping. Interested readers are referred to [33] for a comprehensive knowledge on the feedforward neural network. This neural network can be linearized by Taylor-expansion at the sampling time t_p as follows

$$\begin{aligned} p(t_k) &= a_1(t_p)p(t_{k-1}) + \cdots + a_{n_p}(t_p)p(t_{k-n_p}) \\ &\quad + b_0(t_p)v(t_k) + \cdots + b_{n_v}(t_p)v(t_{k-n_v}) + \zeta(t_p), \end{aligned} \quad (4)$$

where

$$\begin{aligned} a_i(t_p) &= \partial\mathscr{F}(\pi(t_k))/\partial\pi_i(t_k)\big|_{\pi(t_k)=\pi(t_p)}, (i = 1, \cdots, n_a), \\ b_{i'}(t_p) &= \frac{\partial\mathscr{F}(\pi(t_k))}{\partial\varphi_{i'+i}(t_k)}\Big|_{\varphi(t_k)=\varphi(t_p)} (i = n_p + 1, i' = 0, \cdots, n_v), \\ \zeta(t_p) &= p(t_p) - a_1(t_p)p(t_{p-1}) - \cdots - a_{n_p}(t_p)p(t_{p-n_p}) \\ &\quad - b_0(t_p)v(t_p) - \cdots - b_{n_v}(t_p)v(t_{p-n_v}). \end{aligned}$$

Then the jth-step ahead predicted displacement of PEAs can be calculated as follows

$$\begin{aligned} \hat{p}(t_{p+j}) =& (1 + a_1(t_p))\hat{p}(t_{p+j-1}) + (a_2(t_p) - a_1(t_p))\hat{p}(t_{p+j-2}) \\ &+ \cdots - a_{n_p}(t_p)\hat{p}(t_{p+j-n_p-1}) + b_0(t_p)\Delta v(t_{p+j}) \\ &+ \cdots + b_{n_v}(t_p)\Delta v(t_{p+j-n_v}), \quad j = 1, \cdots, N_y, \end{aligned} \quad (5)$$

where $\hat{p}(t_{p+j})$ is the predicted displacement of PEAs, N_y is the prediction horizon and $\Delta v(t_{p+j}) = v(t_{p+j}) - v(t_{p+j-1})$.

By optimizing the following performance index

$$\begin{aligned} &\text{argmin}_{\Delta v(t_{p+1}), \cdots, \Delta v(t_{p+N_y})} \\ &\sum_{j=1}^{N_y} \left((\hat{p}(t_{p+j}) - p_r(t_{p+j}))^2 + \rho(\Delta v(t_{p+j}))^2 \right), \end{aligned} \quad (6)$$

the model predictive controller $v(t_{p+1})$ can be designed $v(t_{p+1}) = v(t_p) + \Delta v(t_{p+1})$, where $p_r(t_p)$ is the desired displacement of PEAs at the pth sampling point and $\rho > 0$ is the penalty parameter for limiting the change of control input. Interested readers are referred to [30] for details in the predictive controller design and the experiment validations.

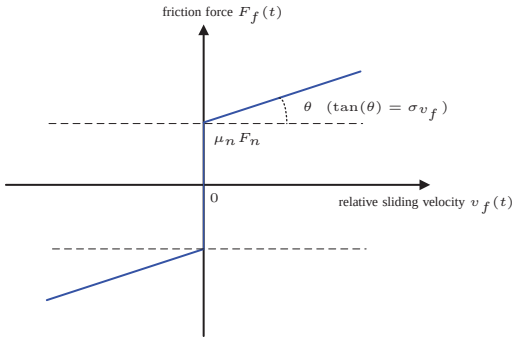

Fig. 4. The "Coulomb + Viscous" friction model.

III. Neural Network Based Positioning Controller of PASSDs

Based on the control paradigm of PASSDs, this section first discusses how to model the relationship between the motion of the end-effector and the motion of the driving object by using neural networks. After that, the inversion of this neural network model has been studied, which can generate the desired motion of the driving object in the sub-step control phase. Finally, the overall positioning controller of PASSDs is presented.

A. End-Effector's Motion Estimator by Neural Networks

For PASSDs, the only driven force of the end-effector is the friction F_f and the motion of the end-effector can be described as follows

$$F_f(t) = M_e \ddot{y}_{ef}(t), \quad (7)$$

where M_e is the mass of the end-effector and $y_{ef}(t)$ denotes the current displacement of the end-effector. By using the "Coulomb + Viscous" friction model shown in Fig. 4, $F_f(t)$ can be written as [34]

$$F_f(t) = \mu_n F_n \text{sign}(v_f(t)) + \sigma_{v_f} v_f(t), \quad (8)$$

where $v_f(t) = d(y(t) - y_{ef}(t))/dt$ denotes the relative sliding velocity between the end-effector and the driving object; sign$(\cdot)$ denotes the sign function; F_n denotes the normal force; μ_n denotes the friction coefficient; σ_{v_f} denotes the viscous friction coefficient.

To determine the motion of the end-effector, an ordinary procedure is to explicitly obtain the friction force and then use this friction to calculate the end-effector's motion. However, equations (7) and (8) reveal that the motion of the end-effector is actually determined by the motion of the driving object/PEA. Therefore, this paper directly obtains the motion of the end-effector by using the following model identification method, which does not need to know the exact values of μ_n, F_n, σ_{v_f} and M_e. Another advantage of this identification-based method is that it is not dependent on the specific form

of the friction model. As long as the friction model indicates that the relationship defined by (9) holds, the proposed identification-based method works. Therefore, the proposed identification-based method can be applied to some cases where the "Coulomb + Viscous" friction model may not be applicable.

By (7) and (8), it is reasonable to believe that $y_{ef}(t)$ is determined by the current and past displacements of the driving object and the past displacements of the end-effector. Therefore, the relationship between the end-effector's motion and the driving object's motion at the sampling times can be written as the following nonlinear auto-regressive moving average with exogenous inputs form

$$y_{ef}(t_k) = \mathscr{F}(y_{ef}(t_{k-1}), \cdots, y_{ef}(t_{k-n_a}), y(t_k), \cdots, y(t_{k-n_b})), \tag{9}$$

where integers n_a and n_b are the corresponding maximum lags for y_{ef} and y, respectively; and $\mathscr{F}(\cdot)$ is the nonlinear mapping which is governed by (7) and (8).

Since the displacement of the end-effector and the displacement of the driving object can be physically collected in experiments, the nonlinear mapping $\mathscr{F}(\cdot)$ can be approximated by the neural-network technique in an off-line manner. In this paper, we also choose the feedforward neural network to approximate the nonlinear mapping $\mathscr{F}(\cdot)$ whose structure is similar with the one shown in Fig. 3. The input-output relationship of the neural network is given as follows:

$$\hat{y}_{ef}(t_k) = \sum_{j=1}^{n} w_j^o \sigma(\sum_{i=1}^{m} w_{ji}^h \varphi_i(t_k) + w_{j0}^h) + w_0^o, \tag{10}$$

where $\hat{y}_{ef}(t_k)$ is the estimated position of the end-effector at the kth sampling point. The number of neurons in the input layer is $m = n_a + n_b + 1$, and n is the number of neurons in the hidden layers. The inputs of this neural-network model are $\varphi_i(t_k)$ ($\varphi_i(t_k)$ is the ith entry of $\varphi(t_k)$, $i = 1, \cdots, m$) and $\varphi(t_k) = (y_{ef}(t_{k-1}), \cdots, y_{ef}(t_{k-n_a}), y(t_k), \cdots, y(t_{k-n_b}))^T$. w_j^o is the weight between the jth hidden neuron and the output neuron; w_0^o is the bias of the output neuron; w_{ji}^h is the weight between the ith input neuron and the jth hidden neuron; w_{j0}^h is the bias of the jth hidden neuron. $\sigma(\cdot)$ denotes the tangent sigmoid function defined by (3).

B. Inversion of the End-effector's Motion Estimator

Equation (9) shows how the end-effector is driven by the driving object via friction, which can be considered as a neural network based forward-motion model. If the inversion of this forward-motion model can be obtained, the desired motion of the driving object/PEA can be calculated by the predesigned motion of the end-effector. To this end, the inversion can be written in the following form

$$\hat{y}(t_k) = \mathscr{F}^{-1}(r_{ef}(t_k), \cdots, y_{ef}(t_{k-n_a}), y(t_{k-1}), \cdots, y(t_{k-n_b})), \tag{11}$$

where $\hat{y}(t_k)$ represents the estimated displacement of the driving object/PEA provided the predesigned position of the end-effector $r_{ef}(t_k)$ and the historic positions of the end-effector and the driving object/PEA.

Since the forward-motion model $\mathscr{F}(\cdot)$ can be approximated by a neural network, its inversion $\mathscr{F}^{-1}(\cdot)$ can also be captured by a neural network. Let $\mathscr{F}^{-1}(\cdot)$ be approximated by the following feedforward neural network

$$\hat{y}(t_k) = \sum_{j=1}^{n} g_j^o \sigma(\sum_{i=1}^{m} g_{ji}^h \phi_i(t_k) + g_{j0}^h) + g_0^o, \tag{12}$$

where and $\phi_i(t_k)$ denotes the ith entry of $\phi(t_k)$. The number of input neuron is $m = n_a + n_b + 1$, then number of hidden neurons is n. g_j^o is the weight between the jth hidden neuron and the output neuron; g_0^o is the bias of the output neuron; g_{ji}^h is the weight between the ith input neuron and the jth hidden neuron; g_{j0}^h is the bias of the jth hidden neuron.

In this paper, this neural-network based inversion model is trained as follows. Given the predesigned position of the end-effector $r_{ef}(t_k)$, the estimated position of the driving object/PEA, $\hat{y}(t_k)$, can be calculated by (12). If the model (12) is an exact inversion of the forward-motion model (10), replacing $y(t_k)$ by its estimated value $\hat{y}(t_k)$ in (10), it can be obtained that the input of (10) becomes $\varphi(t_k) = (y_{ef}(t_{k-1}), \cdots, y_{ef}(t_{k-n_a}), \hat{y}(t_k), y(t_{k-1}), \cdots, y(t_{k-n_b}))^T$. In this case, the output of (10), $\hat{y}_{ef}(t_k)$, should equal to $r_{ef}(t_k)$.

Then the training objective is to adjust the weights g_{ji}^h, g_{j0}^h, g_j^o, g_0^o in (12) such that the square error $e^2(t_k) = (\hat{y}_{ef}(t_k) - r_{ef}(t_k))^2$ is minimized. Since the forward-motion model (10) has been trained well, the weights of the neural network model (10) are fixed. Therefore, the derivatives of $e^2(t_k)$ with respect to these weights can be calculated as follows

$$\begin{aligned}
\frac{\partial e^2(t_k)}{\partial g_{ji}^h} &= \frac{\partial e^2(t_k)}{\partial \hat{y}(t_k)} \frac{\partial \hat{y}(t_k)}{\partial g_{ji}^h}, \\
\frac{\partial e^2(t_k)}{\partial g_{j0}^h} &= \frac{\partial e^2(t_k)}{\partial \hat{y}(t_k)} \frac{\partial \hat{y}(t_k)}{\partial g_{j0}^h}, \\
\frac{\partial e^2(t_k)}{\partial g_j^o} &= \frac{\partial e^2(t_k)}{\partial \hat{y}(t_k)} \frac{\partial \hat{y}(t_k)}{\partial g_j^o}, \\
\frac{\partial e^2(t_k)}{\partial g_0^o} &= \frac{\partial e^2(t_k)}{\partial \hat{y}(t_k)} \frac{\partial \hat{y}(t_k)}{\partial g_0^o},
\end{aligned} \tag{13}$$

where

$$\begin{aligned}
&\frac{\partial \hat{y}(t_k)}{\partial g_0^o} = 1, \\
&\frac{\partial \hat{y}(t_k)}{\partial g_j^o} = \sigma(\sum_{i=1}^{m} g_{ji}^h \phi_i(t_k) + g_{j0}^h), \\
&\frac{\partial \hat{y}(t_k)}{\partial g_{j0}^h} = \sum_{j=1}^{n} g_j^o (1 - \sigma^2(\sum_{i=1}^{m} g_{ji}^h \phi_i(t_k) + g_{j0}^h)), \\
&\frac{\partial \hat{y}(t_k)}{\partial g_{ji}^h} = \sum_{j=1}^{n} g_j^o \phi_i(t_k)(1 - \sigma^2(\sum_{i=1}^{m} g_{ji}^h \phi_i(t_k) + g_{j0}^h)), \\
&\frac{\partial e^2(t_k)}{\partial \hat{y}(t_k)} = 2 \frac{\partial \hat{y}_{ef}(t_k)}{\partial \hat{y}(t_k)} e(t_k), \\
&\frac{\partial \hat{y}_{ef}(t_k)}{\partial \hat{y}(t_k)} = \sum_{j=1}^{n} w_j^o w_{j(n_a+1)}^h \big(1 - \sigma^2(\sum_{i=1}^{m} w_{ji}^h \varphi_i(t_k) + w_{j0}^h)\big).
\end{aligned}$$

Then the training of the inversion model (12) can be made by using the well-known Back-Propagation training method

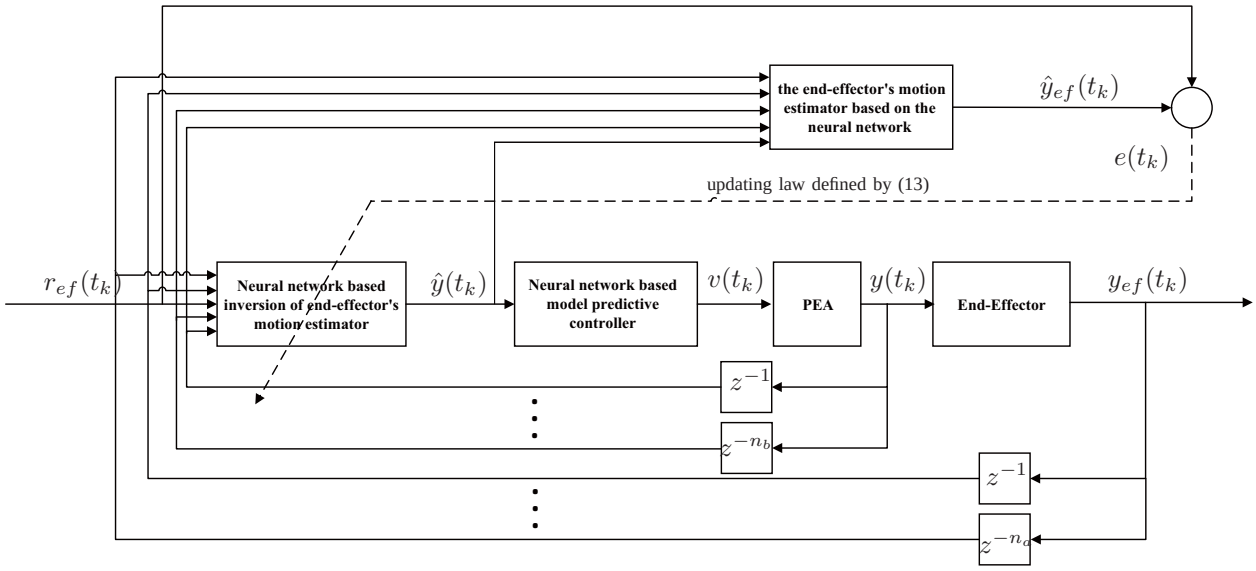

Fig. 5. The schematic of the overall controller in the sub-step control phase: the desired reference $r_{ef}(t_k)$ of the end-effector; the real displacement $y_{ef}(t_k)$ of the end-effector; the estimated displacement $\hat{y}_{ef}(t_k)$ of the end-effector; the desired displacement $\hat{y}(t_k)$ of the driving object/PEA; the input voltage $v(t_k)$ applied to the PEA; the real displacement $y(t_k)$ of the driving object/PEA.

like the Levenberg-Marquardt algorithm [32]. This general idea is similar as the neural network based internal model control approach introduced in the reference [35].

C. Overall Controller of PASSDs

According to (12), the desired displacement of the driving object/PEA can be obtained. The next step is to utilize the dynamic linearized neural network based model predictive controller presented in Section II-B to control the PEA in a fast manner (use $\hat{y}(t_k)$ obtained from (12) to replace the desired reference p_r of PEAs in (6) for calculating the control effort of PEAs). Then the sub-step control phase has been fulfilled. By combining the neural network based inversion of the end-effector's motion estimator and the model predictive control method, the overall control scheme in the sub-step control phase is developed, whose schematic is shown in Fig. 5.

Remark 1: It should be noted that the proposed controller also has some limitations. For example, the proposed method for PASSDs is a kind of data-driven based approach. To determine the neural network based end-effector's motion estimator and its inversion, a large amount of training data must be collected via experiments, and these data can only be used for the controller of the specific PASSD device. If a new PASSD is adopted, the entire training procedure should be re-conducted. In addition, the configuration of the neural network (i.e., the number of hidden neurons and the selection of activation functions) is determined by the trial-and-error approach. Intensive experiments should be made to obtain a satisfactory configuration as well.

IV. Experiments and Discussions

To verify the proposed modeling and control methods, a PASSD prototype is developed and relevant experiments are conducted on this prototype. This prototype is composed of one commercial PEA product (P-753.1CD, Physik Instrumente, Karlsruhe, Germany) and an end-effector. Both the PEA and the end-effector have the "V-shape" grooves as the contact surfaces. Polished silicon wafers are adhered to the "V-shape" grooves of the PEA and the end-effector, respectively. The end-effector is vertically placed on the PEA. The PEA can perform a horizontal motion up to 12 μm, and the displacement measurement of the PEA is realized by a built-in capacitive displacement sensor, which has a high resolution of 0.05nm. In addition, an inductive sensor (SMT 9700, Kaman, Windsor, CT) with a resolution of 0.01 μm is adopted to measure the displacement of the end-effector. An I/O data acquisition board (PCI-1716, Advantech, Beijing, China) is used to exchange the data of the prototype with the host computer. The proposed modelling and control schemes are both realized by SIMULINK with the toolbox of Real-Time Windows Target, and the sampling interval in the following experiments is set to be 0.001s. The PASSD prototype and the experiment setup are presented in Fig. 6.

A. Verification of the End-Effector's Motion Estimator

The performance of the neural network based end-effector's motion estimator is verified by experiments. After training the neural network model (10), the sinusoid waves of 30Hz and 60Hz are applied to the PEA to validate the end-effector's motion estimator. Under this sinusoid signal, there is relative motion between the end-effector and the PEA. The experimental results are given in Figs. 7 and 8. It can be seen that for the excited sinusoid signal of 30Hz, the positioning error of the end-effector's motion estimator is between -0.0411 μm and 0.0431 μm. For the signal of 60Hz, this positioning error increases slightly to [-0.0680, 0.0527] μm. Therefore, the motion of the end-effector can be well described by the proposed neural network model even if the friction force is not directly used to calculate the end-effector's motion.

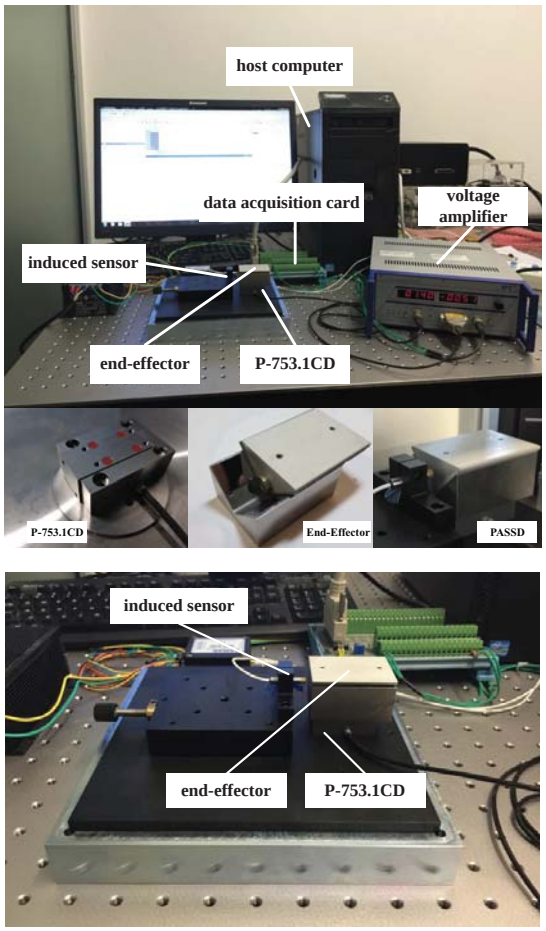

Fig. 6. The PASSD prototype for validating the proposed methods.

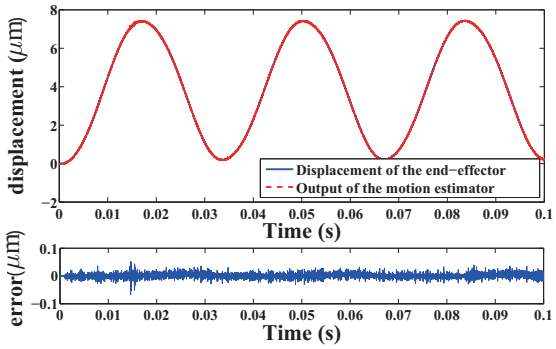

Fig. 7. Performance of the end-effector's motion estimator: the sinusoid signal of 30Hz.

B. Verification of the Model Predictive Controller

For the proposed controller of PASSDs, the dynamic linearized neural network based model predictive control method is employed to handle the control of the PEA in the sub-step control phase. Since the positioning accuracy of the end-effector is directly related to the control performance of this model predictive control method, the following experiment is conducted to verify the effectiveness of the model predictive control method. Here, the periodic and non-periodic signals are both used as the test tracking references. For the periodic

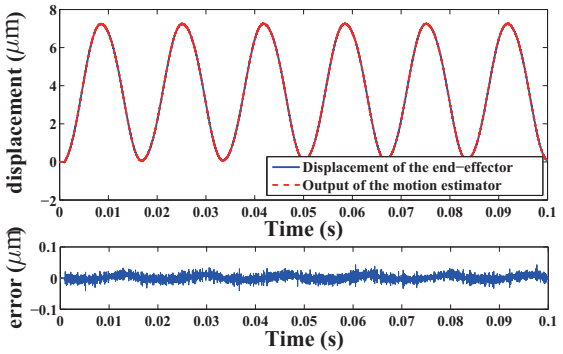

Fig. 8. Performance of the end-effector's motion estimator: the sinusoid signal of 60Hz.

signal, the position tracking error of the PEA is shown in Fig. 9, from which it can be seen that the steady-state tracking error is between -0.0359μm and 0.0331μm. As shown in Fig. 10, the motion of the PEA is seriously affected by the hysteresis nonlinearity in the open loop control mode, while the hysteresis nonlinearity has been well compensated by the model predictive control method. As to the non-periodic reference signal, similar results have been found (as shown in Fig. 12, the steady-state tracking error is $[-0.0348\mu$m, 0.0543μm], and the input-output relationship is nearly linear). These experiments demonstrate that the model predictive controller is an effective one to deal with the control of PEAs in the sub-step control phase.

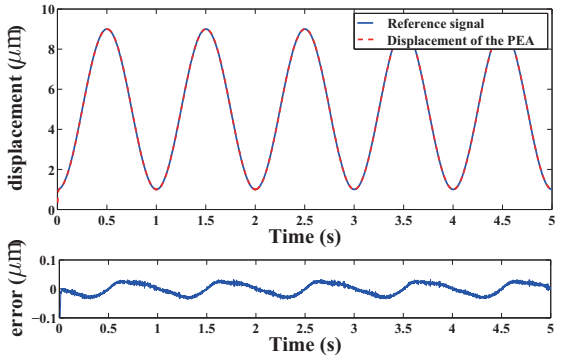

Fig. 9. Performance validation of the model predictive control method under the periodic tracking reference.

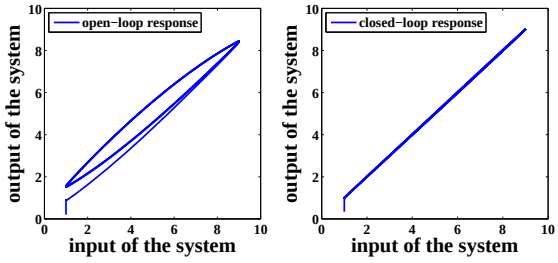

Fig. 10. Input-output relationship of the closed-loop control system: the periodic tracking case.

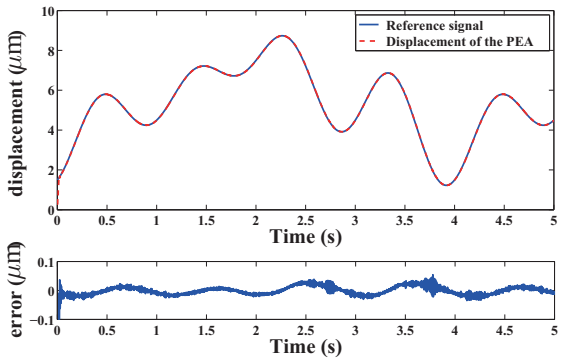

Fig. 11. Performance validation of the model predictive control method under the non-periodic tracking reference.

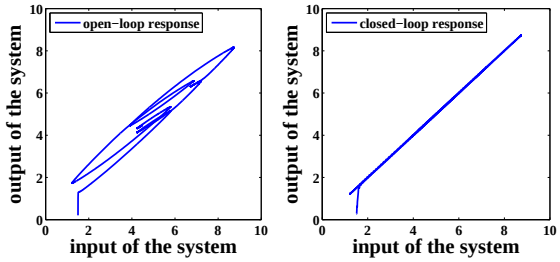

Fig. 12. Input-output relationship of the closed-loop control system: the non-periodic tracking case.

C. Verification of the Neural Network based Control in the Sub-Step Control Phase

To verify the neural network based controller proposed in the sub-step control phase, the following experiments have been conducted on the PASSD prototype. First, a tracking control of a step signal (7μm) is investigated. The experiment results are presented in Fig. 13. It can be seen that the end-effector moves to the reference position in a short time. Meanwhile, the overshoot in the transient phase is very small. Figure 14 gives the motion of the end-effector and the motion of the PEA. It is clear that during the time interval $[0.00\text{s}, 0.01\text{s}]$, there is a relative motion between the end-effector and the PEA, which means that the "zero relative-motion" based controller proposed in [31] does not work and the friction effect must be considered. By the end-effector's motion estimator and its inversion presented in Section III, the neural network based controller proposed in this paper can handle the non-zero relative motion without explicitly using the friction model. From the experiment results shown in Figs. 13 and 14, the end-effector is able to reach the pre-designed set-point 7μm, and this illustrates that the neural network based inversion model (12) of the end-effector's motion estimator can generate a correct position for the PEA and the model predictive controller can ensure the PEA to reach the desired position in a fast manner.

The second experiment verifies the tracking control performance of the proposed controller in the sub-step control phase. Here the sinusoid signal $(3\sin(20\pi t-\pi/2)+3)\mu$m) is adopted as the reference signal of the end-effector. The displacements

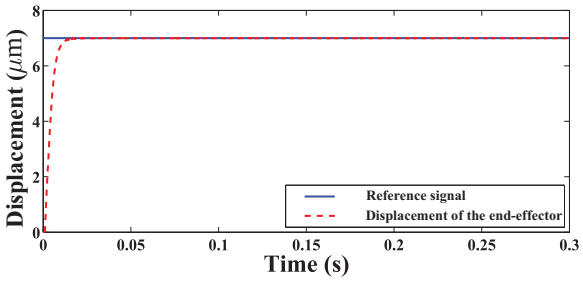

Fig. 13. Positioning control of PASSDs in the sub-step control phase: the step signal 7μm.

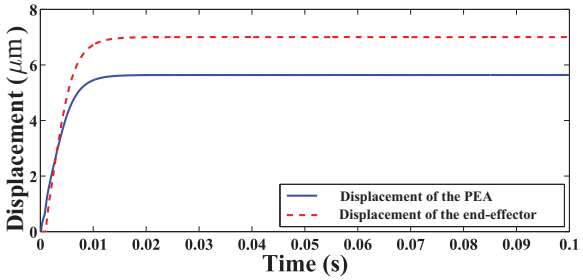

Fig. 14. Displacements of the end-effector and the PEA under the step signal positioning case.

of the end-effector and the PEA are both provided in Fig. 15. It is obvious that the relative motion between the end-effector and the PEA exists. The tracking performance of the proposed controller is given in Fig. 16. It can be seen that the end-effector can still track this time-varying reference signal in a satisfactory way, which demonstrates the effectiveness of the proposed neural network based method.

D. Verification of the Overall Controller of PASSDs

Finally, the overall controller of PASSDs has been verified by experiments. The references of the end-effector are set to be 30μm and 40μm, respectively. For the one-step control phase, the sawtooth signal of 5Hz is chosen as the open loop control input. By the experiment results shown in Fig. 17, after some one-step control phases, the end-effector moves to the position close to the predesigned reference. Then the coarse positioning by the one-step control phase ends and the control system switches to the proposed neural network based controller in the sub-step control phase, which can generate a fine positioning for the end-effector (the steady-state tracking error is smaller than 0.05μm). It is noted that the motion range of the PEA (P-753.1CD) is only 12 μm. By using the PASSD technique, the motion range can be enlarged while the high positioning accuracy remains, which demonstrated the advantage of PASSDs. Through the experiment validation, the proposed overall control method is a promising way to handle the control of PASSDs.

V. Conclusions

In this paper, a neural-network based controller is proposed for the high-precision control of PASSDs. This controller includes two control phases: the one-step control phase and

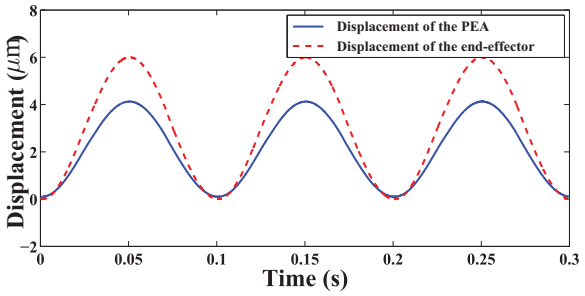

Fig. 15. Displacements of the end-effector and the PEA under the time-varying signal tracking case.

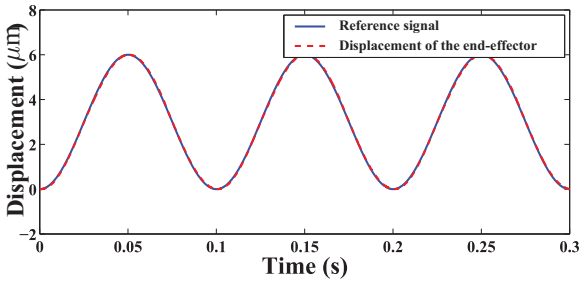

Fig. 16. Time-varying reference tracking performance of the end-effector in the sub-step control phase.

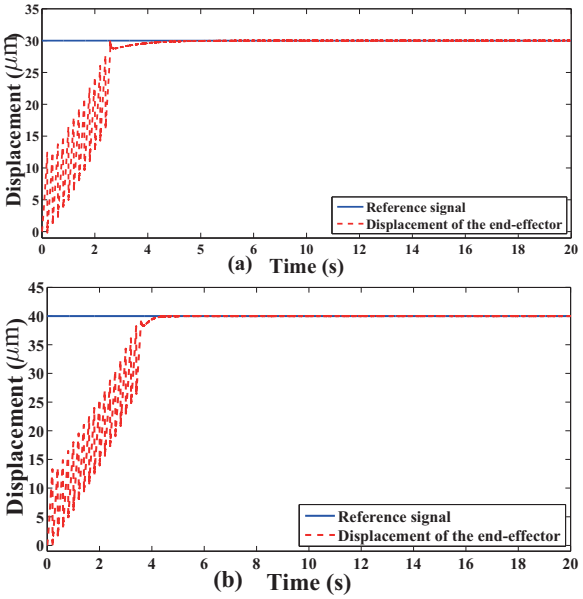

Fig. 17. Positioning performance of PASSDs by the proposed method: (a) the reference 30μm and (b) the reference 40μm.

the sub-step control phase. The one-step control phase belongs to the open-loop control scheme which can only lead to a coarse positioning of PASSDs. And the sub-step control phase requires the displacement feedback of the end-effector and the PEA, which can result in a high-precision positioning of the end-effector. In the sub-step control phase, a neural network based model is first developed to estimate the relative motion between the end-effector and the PEA. Then the inversion of this estimator is designed to calculate the desired position of the PEA by the predesigned reference of the end-effector. Furthermore, the dynamic linearized neural network based model predictive controller is employed to control the PEA to the desired position in a fast manner, and this results in a high-precision controller of PASSDs. The experiments are conducted on a PASSD prototype, and experiment results show that the proposed method is able to control PASSDs with a desired performance.

REFERENCES

[1] W. Yang, S.-Y. Lee, and B.-J. You, "A piezoelectric actuator with a motion-decoupling amplifier for optical disk drives," *Smart Materials and Structures*, vol. 19, no. 6, pp. 065 027.1–065 027.10, May. 2010.

[2] U. Bhagat, B. Shirinzadeh, Y. Tian, and D. Zhang, "Experimental analysis of laser interferometry-based robust motion tracking control of a flexure-based mechanism," *IEEE Transactions on Automation Science and Engineering*, vol. 10, no. 2, pp. 267–275, Apr. 2013.

[3] K. Leang and S. Devasia, "Feedback-linearized inverse feedforward for creep, hysteresis, and vibration compensation in afm piezoactuators," *IEEE Transactions on Control Systems Technology*, vol. 15, no. 5, pp. 927–935, Sept. 2007.

[4] G. Gu, L.-M. Zhu, C.-Y. Su, H. Ding, and S. Fatikow, "Modeling and control of piezo-actuated nanopositioning stages: a survey," *IEEE Transactions on Automation Science and Engineering*, vol. 13, no. 1, pp. 313–332, Jan. 2016.

[5] S. Devasia, E. Eleftheriou, and S. Moheimani, "A survey of control issues in nanopositioning," *IEEE Transactions on Control Systems Technology*, vol. 15, no. 5, pp. 802–823, Sept. 2007.

[6] Y. Wang, J. Zhu, M. Pang, J. Luo, S. Xie, M. Liu, L. Sun, C. Zhou, M. Tan, J. Ge, Y. Sun, and C. Ru, "A stick-slip positioning stage robust to load variations," *IEEE/ASME Transactions on Mechatronics*, vol. 21, no. 4, pp. 2165–2173, Aug. 2016.

[7] Z. Zhang, Q. An, J. Li, and W. Zhang, "Piezoelectric friction-inertia actuator – a critical review and future perspective," *International Journal of Advanced Manufacturing Technology*, vol. 62, no. 5, pp. 669–685, 2012.

[8] M. Hunstig, "Piezoelectric inertia motors – a critical review of history, concepts, design, applications and perspectives," *Actuators*, vol. 6, DOI 10.3390/act6010007, no. 1, 2017.

[9] Y. Liu, X. Hu, Z. Zhang, L. Cheng, Y. Lin, and W. Zhang, "Modeling and control of piezoelectric inertia-friction actuators: review and future research directions," *Mechnical Sciences*, vol. 6, Jul. 2015.

[10] Y. Qin, Y. Tian, D. Zhang, B. Shirinzadeh, and S. Fatikow, "A novel direct inverse modeling approach for hysteresis compensation of piezoelectric actuator in feedforward applications," *IEEE/ASME Transactions on Mechatronics*, vol. 18, no. 3, 2013.

[11] Y. Cao, L. Cheng, X. Chen, and J. Peng, "An inversion-based model predictive control with an integral-of-error state variable for piezoelectric actuators," *IEEE/ASME Transactions on Mechatronics*, vol. 18, no. 3, 2013.

[12] J. Peng and X. Chen, "Integrated pid-based sliding mode state estimation and control for piezoelectric actuators," *IEEE/ASME Transactions on Mechatronics*, vol. 19, no. 1, 2014.

[13] Q. Xu and Y. Li, "Micro-/nanopositioning using model predictive output integral discrete sliding mode control," *IEEE Transactions on Industrial Electronics*, vol. 59, no. 2, 2012.

[14] Q. Xu, "Digital integral terminal sliding mode predictive control of piezoelectric-driven motion system," *IEEE Transactions on Industrial Electronics*, vol. 63, no. 6, 2016.

[15] Q. Xu, "Piezoelectric nanopositioning control using second-order discrete-time terminal sliding mode strategy," *IEEE Transactions on Industrial Electronics*, vol. 62, no. 12, 2015.

[16] W. Liu, L. Cheng, Z.-G. Hou, and M. Tan, "An active disturbance rejection controller with hysteresis compensation for piezoelectric actuators," in *Proceedings of the 12th World Congress on Intelligent Control and Automation*, pp. 2148–2153, Jun. 2016.

[17] W. He, X. He, and C. Sun, "Vibration control of an industrial moving strip in the presence of input deadzone," *IEEE Transactions on Industrial Electronics*, vol. 64, no. 6, 2017.

[18] L. Cheng, W. Liu, Z.-G. Hou, J. Yu, and M. Tan, "Neural network based nonlinear model predictive control for piezoelectric actuators," *IEEE Transactions on Industrial Electronics*, vol. 62, no. 12, 2015.

[19] W. Liu, L. Cheng, Z.-G. Hou, and M. Tan, "An inversion-free model predictive control with error compensation for piezoelectric actuators,"

in *Proceedings of the 2015 American Control Conference*, pp. 5489–5494, Jul. 2015.
[20] W. Liu, L. Cheng, H. Wang, Z.-G. Hou, and M. Tan, "An inversion-free fuzzy predictive control for piezoelectric actuators," in *Proceedings of the 27th Chinese Control and Decision Conference*, pp. 959–964, May. 2015.
[21] L. Cheng, W. Liu, Z.-G. Hou, T. Huang, J. Yu, and M. Tan, "An adaptive takagi-sugeno model based fuzzy predictive controller for piezoelectric actuators," *IEEE Transactions on Industrial Electronics*, vol. 64, no. 6, 2017.
[22] M. Rana, H. Pota, and I. Petersen, "Nonlinearity effects reduction of an afm piezoelectric tube scanner using mimo mpc," *IEEE/ASME Transactions on Mechatronics*, vol. 20, no. 3, 2015.
[23] C. Wen and M. Cheng, "Development of a recurrent fuzzy cmac with adjustable input space quantization and self-tuning learning rate for control of a dual-axis piezoelectric actuated micro motion stage," *IEEE Transactions on Industrial Electronics*, vol. 60, no. 11, 2013.
[24] M. Rakotondrabe, Y. Haddab, and P. Lutz, "Development, modeling, and control of a micro-/nanopositioning 2-dof stick-slip device," *IEEE/ASME Transactions on Mechatronics*, vol. 14, no. 6, 2009.
[25] H. Nguyen, C. Edeler, and S. Fatikow, "Modeling of piezo-actuated stick-slip micro-drives: an overview," *Advances in Science and Technology*, vol. 81, no. 3, 2012.
[26] M. Rakotondrabe, Y. Haddab, and P. Lutz, "Voltage/frequency proportional control of stick-slip micropositioning systems," *IEEE Transactions on Control Systems Technology*, vol. 16, no. 6, 2008.
[27] Q. Zou, C. Giessen, J. Garbini, and S. Devasia, "Precision tracking of driving wave forms for inertial reaction devices," *Review of Scientific Instruments*, vol. 76, Feb. 2005.
[28] M. Spiller and Z. Hurak, "Hybrid charge control for stick-slip piezoelectric actuators," *Mechatronics*, vol. 21, no. 1, 2011.
[29] S. Chao, J. Garbini, W. Dougherty, and J. Sidles, "The design and control of a three-demensional piezoceramic tube scanner with an inertial slider," *Review of Scientific Instruments*, vol. 77, Jun. 2006.
[30] W. Liu, L. Cheng, J. Yu, Z.-G. Hou, and M. Tan, "An inversion-free predictive controller for piezoelectric actuators based on a dynamic linearized neural network model," *IEEE/ASME Transactions on Mechatronics*, vol. 21, no. 1, Feb. 2015.
[31] W. Liu, L. Cheng, C. Zhou, Z.-G. Hou, and M. Tan, "Neural-network based model predictive control for piezoelectric-actuated stick-slip micro-positioning devices," in *Proceedings of IEEE/ASME International Conference on Advanced Intelligent Mechatronics*, pp. 1312–1317, Jul. 2016.
[32] J. Nocedal and S. Wright, *Numerical Optimization (2nd)*. Springer, 1999.
[33] S. Haykin, *Neural Networks: A Comprehensive Foundation (2nd)*. Prentice Hall, 1998.
[34] H. Olsson, K. Åström, C. C. de Wit, M. Gäfvert, and P. Lischinsky, "Friction models and friction compensation," *European Journal of Control*, vol. 4, no. 3, 1998.
[35] K. Hunt and D. Sbarbaro, "Adaptive filtering and neural networks for realisation of internal model control," *Intelligent Systems Engineering*, vol. 2, no. 2, 1993.

Long Cheng (SM'14) received the B.S. degree (with honors) in control engineering from Nankai University, Tianjin, China, in July 2004, and the Ph.D. degree (with honors) in control theory and control engineering from the Institute of Automation, Chinese Academy of Sciences, Beijing, China, in July 2009. Currently, he is a full professor at the Laboratory of Complex Systems and Intelligent Science, Institute of Automation, Chinese Academy of Sciences. Dr. Cheng is also an adjunct professor at University of Chinese Academy of Sciences. His current research interests include intelligent control of smart materials, coordination of multi-agent systems, neural networks and their applications to robotics.

Weichuan Liu received the B.E. degree in control engineering from North China University of Technology, Beijing, China, in July 2013, and the Ph.D. degree in control theory and control engineering at Institute of Automation, Chinese Academy of Sciences, Beijing, China, in July 2016. Currently, he is a research scientist at IBM China Development Lab. His research interests include predictive control, intelligent control and nano/micro robots.

Chenguang Yang (SM'16) received the B.Eng. degree in measurement and control from Northwestern Polytechnical University, Xi'an, China, in 2005, and the Ph.D. degree in control engineering from the National University of Singapore, Singapore, in 2010. He received postdoctoral training at Imperial College London, UK. He is with Zienkiewicz Centre for Computational Engineering, Swansea University, UK as a senior lecturer. His research interests lie in robotics, automation and computational intelligence.

Tingwen Huang (M'12) is a Professor at Texas A&M University at Qatar. He received his B.S. degree from Southwest Normal University (now Southwest University), China, 1990, his M.S. degree from Sichuan University, China, 1993, and his Ph.D. degree from Texas A&M University, College Station, Texas, 2002. After graduated from Texas A&M University, he worked as a Visiting Assistant Professor there. Then he joined Texas A&M University at Qatar (TAMUQ) as an Assistant Professor in August 2003, then he was promoted to Professor in 2013. Dr. Huang's focus areas for research interests include neural networks, chaotic dynamical systems, complex networks, optimization and control.

Zeng-Guang Hou (SM'09) received the B.E. and M.E. degrees in electrical engineering from Yanshan University (formerly North-East Heavy Machinery Institute), Qinhuangdao, China, in 1991 and 1993, respectively, and the Ph.D. degree in electrical engineering from the Beijing Institute of Technology, Beijing, China, in 1997. He is now a Professor in the State Key Laboratory of Management and Control for Complex Systems, Institute of Automation, Chinese Academy of Sciences. His current research interests include neural networks, optimization algorithms, robotics, and intelligent control systems.

Min Tan received the B.S. degree in control engineering from Tsinghua University, Beijing, China, in 1986 and the Ph.D. degree in control theory and control engineering from Institute of Automation, Chinese Academy of Sciences, Beijing, in 1990. He is a Professor in the Laboratory of Complex Systems and Intelligent Science, Institute of Automation, Chinese Academy of Sciences. His research interests include advanced robot control, multirobot systems, biomimetic robots, and manufacturing systems.